

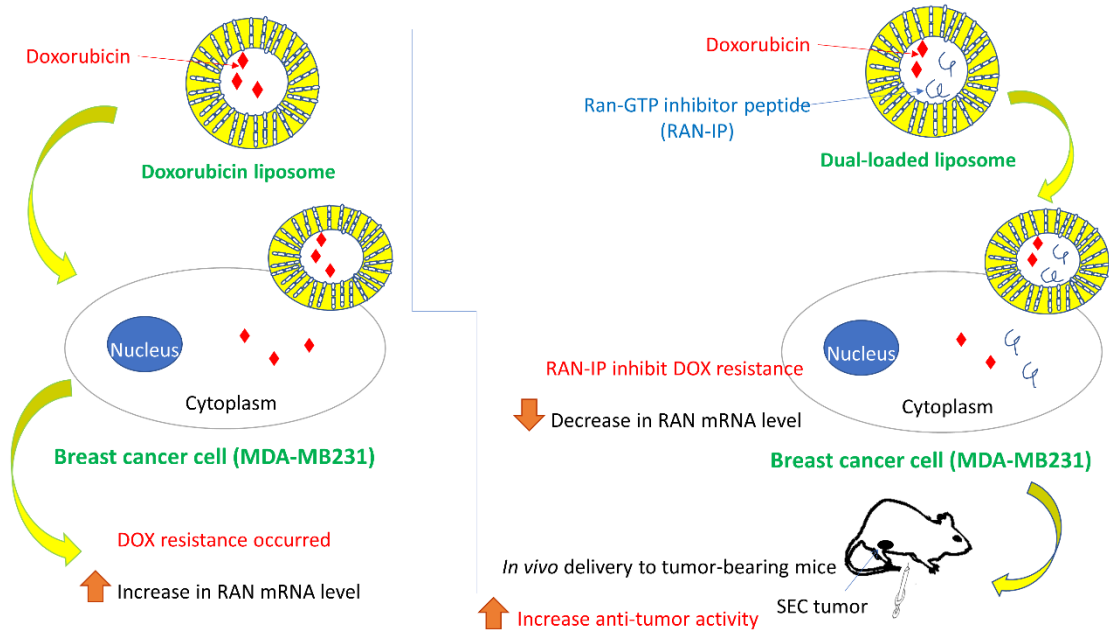
# bradscholars

## Co-delivery of a RanGTP inhibitory peptide and doxorubicin using dual loaded liposomal carriers to combat chemotherapeutic resistance in breast cancer cells

Item Type	Article
Authors	Haggag, Y.;Abu Ras, Bayan;El-Tanani, Yahia;Tambuwala, M.M.;McCarron, P.;Isreb, Mohammad;El-Tanani, Mohamed
Citation	Haggag Y, Abu Ras B, El-Tanani Y et al (2020) Co-delivery of a RanGTP inhibitory peptide and doxorubicin using dual loaded liposomal carriers to combat chemotherapeutic resistance in breast cancer cells. Expert Opinion on Drug Delivery. 17(11): 1655-1669.
DOI	<a href="https://doi.org/10.1080/17425247.2020.1813714">https://doi.org/10.1080/17425247.2020.1813714</a>
Rights	© 2020 Taylor & Francis. This is an Author's Original Manuscript of an article published by Taylor & Francis in Expert Opinion on Drug Delivery on 15 Sep 2020 available online at <a href="https://doi.org/10.1080/17425247.2020.1813714">https://doi.org/10.1080/17425247.2020.1813714</a> .
Download date	2026-05-12 13:19:37
Link to Item	<a href="http://hdl.handle.net/10454/18020">http://hdl.handle.net/10454/18020</a>

# 1 Graphical Abstract

2



3

4

## 5 **1-Introduction**

6 Breast cancer is a genetic disease, characterized by gene mutation, rearrangement,  
7 and amplification [1]. High mortality rates in industrialized countries are well documented  
8 [2], along with the limitations and adverse effects associated with the various protocols  
9 used during treatment [3]. It is a heterogeneous disease with several subtypes based on the  
10 expression of three different receptors, namely the progesterone, estrogen, and human  
11 epidermal growth factor receptor 2 (HER-2/neu)[4]. Clinical options share much with  
12 conventional chemotherapeutic strategies, based on the administration of cytotoxic drugs  
13 as a first-line approach, as is often the case with other types of cancer [5]. However, these  
14 types of regimens frequently induce multidrug resistance (MDR), leading to significant  
15 limitations in clinical outcomes [6]. MDR can develop over multiple rounds of continual  
16 chemotherapy and via various molecular mechanisms, including the regulation and  
17 deregulation of drug influx [7], mutation of drug targets, activation of DNA repair  
18 mechanisms, and deregulation of apoptosis [8].

19 Doxorubicin (DOX) is considered an orthodox chemotherapeutic drug. It is  
20 frequently used to treat solid tumors, such as breast, lung, gastric, ovarian, and thyroid  
21 cancers. The clinical use of DOX is limited severely by the risk of progressive, dose-  
22 dependent cardiomyopathy, and irreversible congestive heart failure [9,10]. There are  
23 considerable efforts in the field of DOX research on maintaining drug efficacy while  
24 reducing toxicity. It is administered as a monotherapy or, more commonly, in combination  
25 with other drugs and is primarily used in breast cancer treatment[11]. Its cytotoxic effect  
26 arises from inhibition of DNA topoisomerase II [12]. Unfortunately, the results of several  
27 studies have linked poor prognosis during DOX treatment with increased MDR [13]. For

28 example, it has been shown that cancer cells evade the apoptotic effect of P53 by  
29 transporting it to the cytoplasm using a CRM1-mediated export mechanism[14].

30         Achieving an effective anti-tumor effect requires an understanding of the MDR  
31 pathway, prompting the development of attenuation strategies based on some form of  
32 interruptive intervention. A decrease of MDR, combined with the simultaneous use of a  
33 potent chemotherapeutic agent, is a potentially advantageous therapeutic strategy [15].  
34 One approach has focused on novel delivery methods, such as anthracycline nano-delivery  
35 systems, reported circumventing MDR effectively, both *in vitro* and *in vivo*[16,17]. This  
36 approach augments the therapeutic effect, whilst minimizing the expected adverse effects  
37 of high drug dosing [18]. Liposomes are of particular interest, having been successfully  
38 employed for the delivery of DOX. They possess a unique bilayer vesicular structure,  
39 comprising an internal aqueous compartment entrapped by one or more concentric lipid  
40 bilayers to facilitate the encapsulation of both lipophilic and hydrophilic drugs[19].  
41 Liposomes have a number of beneficial properties, when compared to other nanosystems  
42 [20,21]. These properties include improving drug solubility, stability, and delivery to  
43 specific target sites [21]. Their sub-cellular size and lipid structure allow for higher  
44 intracellular uptake, which improves drug bioavailability when compared to other  
45 particulate systems. Furthermore, they provide drug protection against degradation while  
46 sustaining its release[20]. The main reason for selecting liposome as a drug nanocarrier is  
47 its significant role in effective drug delivery to target sites while minimizing systemic  
48 toxicity. Liposomal formulations have been shown to be beneficial for stabilizing  
49 therapeutic biomolecules, overcoming obstacles of cellular and tissue uptake, and  
50 improving the drug biodistribution to target sites *in vivo*. Liposomes exhibited positive

51 outcomes in preclinical studies, thus the clinical translation of liposome-based drug  
52 delivery platforms has improved incrementally[22].

53 Our group has a particular interest in the functions of Ras-related nuclear protein  
54 (Ran). It is a key component of the exportin transport system and exists in two nucleotide  
55 forms [16]. It is best known for its roles in directional nucleocytoplasmic transport, mitotic  
56 spindle fiber assembly, and post-mitotic nuclear envelope dynamics[23]. Ran  
57 overexpression induces cellular transformation, tumorigenesis, and metastasis, both *in*  
58 *vitro* and *in vivo*[24,25]. Cancer cells with mutations and abnormal expression in proto-  
59 oncogenes and suppressors correlate to the activation of the PI3K/Akt/mTORC1 and  
60 Ras/MEK/ERK pathways, which are the most frequently dysregulated signaling pathways  
61 in cancer[26]. These pathways are more susceptible to Ran knockdown than normal cells  
62 [27,28].

63 The cellular compartmentalization of the Ran GTP-GDP cycle is regulated by the  
64 Ran guanine nucleotide exchange factor (RCC1). Besides, Ran-GAP creates a Ran-GTP  
65 gradient, which controls the transport of macromolecules between the nucleus and the  
66 cytoplasm [26]. RanGTP-regulated nuclear export and import pathways control the cell  
67 cycle rate and cellular responses to DNA damage. If the cellular RanGTP concentration  
68 reaches a threshold, RanGTP-regulated nuclear-cytoplasmic transport reactions approach  
69 rates that support normal DNA Damage Response (DDR) function and cell cycle  
70 transitions. Consequently, DNA damage in such cells is successfully repaired, followed by  
71 termination of DDR and re-entry into the cell cycle. If RanGTP levels fall below the  
72 required threshold or a required nuclear transport receptor pathway is defective, the  
73 mechanisms of DNA repair or cell cycle re-entry are delayed. This, in turn, triggers cell

74 cycle arrest or possible cell death [29]. The relation between Ran gene and DOX is  
75 controlled by the role of RCC-1. It was reported that, RCC1 promotes doxorubicin  
76 resistance in colorectal carcinoma cells. Besides, overexpression of RCC1 prevented the  
77 onset of DNA damage-induced cell senescence in normal cells. In case of colonic  
78 carcinoma, RCC1 overexpression strongly increased cell survival following doxorubicin-  
79 induced DNA damage. RCC1 overexpression was sufficient to accelerate cell cycle and  
80 DNA damage repair after DOX treatment[30].

81 Our group has reported previously, for the first time, on a specific peptide segment  
82 (CAQPEGQVQFK), known as Ran-RCC1 inhibitory peptide (RAN-IP). Its structure is  
83 based on the Ran protein sequence and blocks the interaction between RanGDP and RCC1  
84 in MDA-MB231 breast cancer cells and A549 lung cancer cells. This competitive  
85 inhibition of the binding of RCC1 to its specific binding pocket present in the RanGDP  
86 conformation prevents RanGTP formation[23,31]. Experimental disruption of the guanine  
87 nucleotide cycle by RAN-IP has been demonstrated using RAN-IP-loaded nanoparticles,  
88 which prevent the generation of RanGTP by disrupting nucleotide-binding with RCC1,  
89 resulting in a dominant inhibitory effect on RanGTP formation. This suppresses  
90 tumorigenesis and metastasis both *in vitro* and *in vivo* [23,31].

91 Herein, we report on a novel liposome-based co-delivery of DOX and RAN-IP as  
92 combination chemotherapy for the first time. Importantly, the delivery of liposomal  
93 payloads comprising combinations of cytotoxic and peptide drugs has been reported  
94 elsewhere, such as paclitaxel and sorafenib, for reversion of multidrug resistance *in vitro*  
95 in breast cancer cells[32]. However, the peptide-based payload is used primarily for  
96 targeting purposes and decorates the peripheral aspects of the liposome, as demonstrated

97 by the co-delivery of DOX and vincristine for the treatment of glioma[33], DOX and  
98 erlotinib for treatment of glioblastoma[34] and DOX for treatment of lung metastasis[35].

99         The first aim of this work was to study the formulation and optimization of the  
100 physicochemical properties of liposomes loaded with both peptide and DOX using  
101 different formulation variables. The second aim was to use simultaneous liposomal  
102 delivery of DOX and RAN-IP to confirm the effect of reducing or reversing the  
103 overexpression of Ran during exposure to DOX. *In vitro* cytotoxicity of these dual  
104 functionalized liposomes was tested on breast and lung cancer cell lines (MDA-MB231,  
105 MCF-7, and A549). Finally, the study aimed to confirm that the upregulation of Ran in  
106 DOX-treated cells, *in vitro*, is a key mechanism that counteracts antineoplastic effects. The  
107 anti-tumor activity of dual functionalized liposomes was evaluated in an *in vivo* Solid  
108 Ehrlich Carcinoma (SEC) breast cancer model.

## 109 **2. Materials and Methods**

### 110 *2.1. Materials*

111 1,2-Dipalmitoyl-sn-glycerol-3-phosphate-rac-(1-glycerol) (DPPG, sodium salt) and 1,2-  
112 dioleoyl-sn-glycerol-3-phosphoethanolamine (DOPE, purity >99%) were purchased from  
113 Avanti Polar Lipids, Inc., (Alabaster, AL). Peptide (NT 3-12) (MW 1243 Da, purity  $\geq$  96%)  
114 was synthesized by GL-Biochem Ltd. (Shanghai, China). Doxorubicin hydrochloride  
115 (DOX), cholesterol, methanol, dichloromethane, and phosphate-buffered saline were  
116 obtained from Sigma-Aldrich Company Ltd. (Poole, UK). Dichloromethane, acetonitrile,  
117 and trifluoroacetic acid were of HPLC grade and other reagents were of analytical grade.  
118 Water used in the work was produced to Type 1 standard (Milli-Q<sup>®</sup>, resistance of 18.2 M $\Omega$   
119 cm at 25 °C, conductivity is < 10  $\mu$ S/cm, ion-free water at the sub-ppb level, total organic  
120 carbon is < 30  $\mu$ g/ml, and pH of 6.99).

121

### 122 *2.2. Preparation of drug-loaded liposomes*

123 Liposomes were prepared using a modified, thin-film rehydration method [36].  
124 Phospholipids and cholesterol (DPPG: DOPE: cholesterol) of (4:4:2 molar ratio) were  
125 dissolved in dichloromethane and methanol (3:1 v/v) in round bottom glassware. The  
126 organic solvent was evaporated at 40 °C using rotary evaporation. The resultant thin film  
127 was maintained under vacuum for 6 hours to ensure removal of residual solvents. The thin  
128 film was hydrated in a solution of NT 3-12 peptide in PBS for 1 hour at 60 °C using a bath  
129 sonication (150 W). The sample was frozen at -20 °C and then a freeze-thaw cycle repeated  
130 four times using bath sonication without addition of cryoprotectant. The sample was  
131 centrifuged at 22,000 g for 30 minutes at 4 °C for purification and removal of the non-

132 encapsulated drug. DOX-loaded liposomes were prepared using this method, differing only  
133 in the rehydration step, where a PBS solution containing dissolved DOX was used. Dual-  
134 loaded liposomes containing both peptide and DOX were prepared using an identical  
135 procedure, but with a PBS solution containing dissolved NT 3-12 peptide and DOX for  
136 rehydration of the lipid film. Process variables, such as the pH of the dispersion medium,  
137 peptide loading and addition of DOX, are listed in (Table 1), together with the identifying  
138 code used to label each liposome formulation.

139

### 140 ***2.3. Characterisation of drug-loaded liposomes***

141 Average size and population spread (polydispersity index) of liposome preparations were  
142 determined using dynamic light scattering (Nanosizer ZS, Malvern Instruments, UK). The  
143 particle size and distribution were measured after each freeze-Thaw cycle during  
144 preparation and after each week for one month during storage for measuring *in vitro*  
145 stability. Liposomal charge (Zeta potential) was determined using laser Doppler  
146 anemometry after a 5-fold dilution in distilled water (Nanosizer ZS, Malvern Instruments,  
147 UK). All measurements were performed in triplicate. Liposomal surface morphology was  
148 studied using transmission electron microscopy (JOEL JEM 2000 EX200) operating at an  
149 accelerating voltage of 80 kV. Samples were prepared by placing a suspension on a  
150 Formvar-coated grid and coating with a carbon layer (20 nm) under vacuum before  
151 scanning.

152

### 153 ***2.4. Determination of drug encapsulation efficiency***

154 Peptide content was determined by an indirect procedure based on the determination of  
155 uncoated free peptide in the supernatant using HPLC [23,31]. Briefly, reversed-phase  
156 chromatography (Phenomenex- Luna<sup>®</sup> C18-5 column mm, 5  $\mu$ m) with a flow rate of 1.0  
157 ml per min, and UV detection (254 nm) was used. A mobile phase elution gradient was  
158 used, comprising two solvent mixtures (solvent A: 0.1% TFA in acetonitrile; solvent B:  
159 0.1% TFA in water). Peptide encapsulation inside the liposome was calculated from the  
160 difference between the initial amount of peptide added and the free peptide remaining in  
161 the supernatant after liposome fabrication. DOX was detected using HPLC performed  
162 under conditions described elsewhere [37]. Chromatographic separation was accomplished  
163 with a mobile phase consisting of acetonitrile: water at a ratio of 30:70 (pH 3.0), and the  
164 drug was detected at 233 nm using a UV detector at a flow rate of 1.0 ml per min and  
165 ambient temperature. Each sample was assayed in triplicate and loading of both peptide  
166 and DOX reported as a percentage encapsulation efficiency (%E.E). **Physicochemical**  
167 **characterizations of peptide-loaded, DOX-loaded and dual-loaded liposomes were**  
168 **represented in (Table 2).**

169

### 170 ***2.5 In vitro release studies***

171 A sample of peptide-loaded liposome formulation containing predetermined amounts of  
172 peptide and DOX was placed into a dialysis bag (10 kDa molecular weight cut off). The  
173 membrane was dialyzed against receptor media (50 ml PBS, pH 7.4). The release was  
174 studied at 37 °C at 100 rpm. At predetermined time interval points, a sample was removed  
175 (1.0 ml) replaced by an equal volume of fresh media to maintain sink conditions. Drug  
176 concentrations were assessed using HPLC, as described previously.

177 **2.6. Cell culture**

178 Breast cancer cell lines (MCF-7 and MDA-MB-231) and non-small cell lung carcinoma  
179 cells (A549) were obtained from the Cell Culture Department, VACSERA (Cairo, Egypt).  
180 Cells were routinely grown in T75 canted-neck tissue culture flasks. Cells were cultured in  
181 Dulbecco's Modified Eagle's Medium (DMEM) medium (Invitrogen/ Life Technologies,  
182 Grand Island, NY) supplemented with FBS (10% v/v), 10 $\mu$ g ml<sup>-1</sup> of insulin and 1%  
183 penicillin-streptomycin. The medium renewal was carried out every three days at 80%  
184 confluence. Cell cultures were incubated at 5% CO<sub>2</sub> and 37 °C.

185

186 **2.7. In vitro cell viability assay**

187 A cell viability assay was performed using an *in vitro* toxicology assay kit (MTT, 7H258,  
188 Sigma, Saint Louise, Missouri, USA) [38,39]. MCF-7, MDA-MB-231, and A549 cells  
189 (1.2-1.8 x10<sup>4</sup> cells/well in 100  $\mu$ l media) were seeded in 96-well plates for 24 hours before  
190 treatment. The following day, all cells were treated with 100  $\mu$ l of each of the following  
191 formulations: blank liposome, free peptide (1  $\mu$ M), free DOX (1  $\mu$ M), peptide-loaded  
192 liposome (1  $\mu$ M), DOX-loaded liposome (1  $\mu$ M), combination of both peptide-loaded  
193 liposome (1  $\mu$ M) and DOX-loaded liposome (1  $\mu$ M), dual-loaded liposome at three  
194 different concentrations (0.25, 0.5 and 1  $\mu$ M). All treatments were suspended in  
195 transfection Optimem<sup>®</sup> media. Untreated MCF-7, MDA-MB-231, and A549 cells were  
196 used as controls.

197 Cell viability following each treatment was determined after 24, 48, and 72 hours.  
198 Treated cells were washed in PBS (100  $\mu$ l) and 100  $\mu$ l of reconstituted MTT (M-5655) dye  
199 solution in complete media was added to each well. The plates were incubated at 37 °C and

200 5% CO<sub>2</sub> for an additional 3 hours. The supernatant was discarded, solubilizing solution  
201 added (M-8910, 100 µl) and gently mixed in to dissolve the precipitate. The color intensity  
202 was measured at 570 nm and the background absorption measured at 690 nm in a  
203 microplate reader (Fluostar Omega, BMG Lab Tech GMBH, Germany). The anti-  
204 proliferative effect of different doses of free drugs and liposomal treatments was calculated  
205 as a percentage of cell growth concerning control cells. The absorbance of the untreated  
206 cells was set at 100%. The dose-effect curves were plotted for each treatment to measure  
207 the drug concentration that caused 50% growth inhibition (IC<sub>50</sub>)[40,41]. All experiments  
208 were performed in triplicate.

209

## 210 ***2.8. Real-time polymerase chain reaction***

211 RNA was extracted using selective binding to silica-based membranes (RNeasy® Mini  
212 Kit, Qiagen Ltd., Manchester, UK), and reverse transcription was performed using  
213 SuperScript™ III first-strand synthesis system (Invitrogen Ltd.) according to the  
214 instructions supplied by the manufacturer. Real-time PCR (Applied Biosystem, Foster  
215 City, CA) was performed using an SYBR® Green assay for RanGTP and a forward primer  
216 5' CCATCTTTCCAGCCTCAGTC 3' and reverse primer 5'  
217 CCAAGGAAGGCGTCTAAGGC 3'.

218

## 219 ***2.9. In vivo study***

### 220 ***2.9.1. Animals***

221 The *In vivo* study was performed on 60 female BALB/C mice, aged 7–8 weeks, and  
222 weighing 20 ± 2 g. They were housed in stainless steel mesh cages in ten groups of six.

223 Mice were kept under standard conditions of light, relative humidity, and temperature, for  
224 ten days before the experiment. Animals had free access to standard laboratory food and  
225 water throughout the study. All procedures were performed according to a protocol  
226 approved by the Faculty of Pharmacy, Tanta University, and designed by the Animal Care  
227 and Use Committee.

228

### 229 ***2.9.2. Development of tumor model***

230 The induction of a solid Ehrlich carcinoma tumor was performed as previously described  
231 [23,42]. Ehrlich ascites tumor (EAT) cells, supplied from the National Institute of Cancer,  
232 Egypt, were collected from the ascites fluid of female mice harboring 8–10-day old ascites  
233 tumor. Approximately,  $2 \times 10^6$  viable EAT cells were suspended in PBS and injected  
234 subcutaneously into the back of BALB/C female mice. Growth was assessed daily until the  
235 tumor volume reached  $100 \text{ mm}^3$ . Volume was calculated by measuring both perpendicular  
236 diameters of the tumor using a digital caliper and applying the following equation [43].

$$237 \quad \text{tumour volume (mm}^3\text{)} = 0.52 \cdot \text{length} \cdot \text{width}^2$$

### 238 ***2.9.3. In vivo antitumor efficacy***

239 To assess the *in vivo* antitumor efficacy of liposome formulations, animals were randomly  
240 separated into ten groups (six mice per each group). The study design of the *in vivo*  
241 experiment and treatment protocols are shown in (Table 3). The tumor-bearing mice were  
242 subdivided into groups, with each receiving an intraperitoneally administered dose every  
243 three days for 16. At the end of the experiment, animals were sacrificed by cervical  
244 dislocation. The excised tumors were washed in cold saline, then weighed to determine the  
245 final tumor weight.

246

## 247 **2.10. Biochemical Assays**

248 Lipid peroxide content in the heart tissue of treated animals was determined by measuring  
249 MDA (Biodiagnostic Ltd., Giza, Egypt). The method used colorimetric detection of the  
250 colored product formed following the reaction between thiobarbituric acid and the MDA  
251 content in heart tissue samples [44]. The assay procedures were conducted according to the  
252 protocol supplied by the manufacturer.

253 Serum lactate dehydrogenase (LDH) was measured by using a LDH kit  
254 (SPINREACT, Spain), following a method previously described [45]. Creatinine kinase  
255 (CK-MB) activity was measured using a propriety assay (Egyptian Company for  
256 Biotechnology, Cairo, Egypt) according to methods described elsewhere [46]. All serum  
257 samples were collected immediately before animal sacrifice.

258

## 259 **2.11. Statistical Analysis**

260 Results for *in vitro* experiments were determined as mean  $\pm$  SD and results from *in vivo*  
261 experiment were presented as mean  $\pm$  SEM. The level of significance was evaluated  
262 statistically using a one-way ANOVA, followed by the post-hoc Tukey's test.  $P < 0.05$  was  
263 considered to be statistically significant for both *in vitro* and *in vivo* experiments.

264

### 265 **3. Results and Discussion**

266 Herein, we used thin film rehydration method followed by freeze-thaw cycle for  
267 preparation of drug-loaded liposomes. Thin film rehydration technique was adopted for  
268 encapsulation of hydrophilic drugs due to its simplicity, reproducibility, practicability, and  
269 its ability to yield small and uniform drug loaded liposomes after freeze-thaw  
270 cycles[47,48].

#### 271 ***3.1. Effect of pH of the dispersion medium***

272 The physicochemical characteristics of three different peptide-loaded liposome  
273 formulations (F1, F2, and F3) are shown in (Table. 2). NT 3-12 peptide was dissolved in  
274 aqueous dispersion media with each adjusted to one of the following pH values (PBS pH  
275 7.4, phosphate buffer pH 6.8, and phosphate buffer pH 6) to investigate the effect of the  
276 pH value on the physicochemical properties of the peptide-loaded liposomes. Decreasing  
277 the pH of the aqueous dispersion medium resulted in a significant increase in liposomal  
278 size. The average size of (F1) rehydrated by phosphate buffer (pH 6) was found to be  $139$   
279  $\pm 21$  which was significantly bigger ( $p < 0.01$ ) compared to  $81 \pm 11$  nm in the case of (F3)  
280 prepared at higher pH of 7.4. Low pH values cause the protonation of the phospholipid  
281 heads and therefore hydrogen bond formation may occur resulting in bigger liposomal size  
282 meanwhile some phospholipid may exhibit electrostatic repulsion between protonated  
283 phospholipid heads. In the case of DPPG, protonation of phospholipid heads was more  
284 likely to occur compared to other lipids so that hydrogen bond formation between adjacent  
285 protonated heads predominate the electrostatic repulsion resulting in larger liposome size  
286 [49,50]. The change in pH value of the dispersion medium showed a slight change in zeta

287 potential ( $p > 0.05$ ). This might be attributed to the poor electrostatic repulsion effect  
288 resulted from the change in pH values.

289 Increasing pH value from 6 to neutral 7.4 resulted in a significant increase in peptide  
290 encapsulation efficiency. The average % E.E of (F1) prepared at a low pH value of 6 was  
291 found to be  $52.13 \pm 7.96$  which was significantly lower than % E.E of  $93.15\% \pm 6.1\%$  in  
292 case (F3) prepared at higher pH of 7.4 ( $p < 0.001$ ). This can be explained by the hydrogen  
293 bond formation between neighbouring protonated heads of DPPG at lower pH which  
294 decreases their hydrophilicity. This subsequently decreases the hydration of the lipid film  
295 by the aqueous drug-containing medium leading to a lower encapsulation efficiency. On  
296 the other hand, smaller liposome size resulted at pH 7.4 exhibited higher surface area  
297 available for lipid hydration with aqueous drug-medium resulting in a higher percentage of  
298 peptide encapsulation[49,50].

299 *In vitro* release profiles of different peptide-loaded liposomes (F1, F2, and F3) showed a  
300 significant decrease ( $p < 0.05$ ) in initial burst release phase in the case of F3 compared to  
301 both F1 and F2 (Fig. 1A). Burst release after 24 h was  $59.17\% \pm 8.36\%$ ,  $53.13\% \pm 5.11\%$ ,  
302 and  $44.66\% \pm 5.7\%$  in case of F1, F2 and F3, respectively. This lower initial burst is  
303 preferable especially in case of *in vivo* administration of nano-drug delivery system  
304 reducing the risk of premature drug release before reaching the targeted site of action [31].

305

### 306 **3.2. Effect of peptide loading**

307 The physicochemical properties of the three peptide-loaded liposome formulations (F3, F6,  
308 and F9) were recorded in (Table 2). Three peptide loadings levels (3%, 5%, and 7% w/w)  
309 were used in this study while maintaining the lipid composition and concentration.

310 Increasing peptide loading resulted in a significant increase in the liposomal size ( $p < 0.05$ ).  
311 liposome size increased from  $81 \pm 11$  nm in the case of 3% w/w peptide loading (F3) to  
312  $128 \pm 14$  nm in the case of 7% w/w peptide loading (F9) ( $p < 0.01$ ). Increasing the peptide  
313 loading might have resulted in the separation of the concentric lipid bilayers encapsulating  
314 the aqueous drug core due to the high molecular weight of the dissolved peptide leading to  
315 the increasing of liposomal surface area and therefore size [51]. The lower level of peptide  
316 loading of 3% w/w (F3) showed a significant decrease in polydispersity compared to a  
317 higher peptide loading level of (F7) ( $p < 0.05$ ). Peptide loading showed no significant effect  
318 on the zeta potential of the liposomes ( $p > 0.05$ ).

319 On the other hand, drug loading had a significant impact on the encapsulation efficiency  
320 of peptide inside liposomes. The increase in peptide loading resulted in a significant  
321 decrease in encapsulation efficiency ( $p < 0.05$ ). Results showed that encapsulation  
322 efficiency observed for F7 was significantly decreased to  $64.7\% \pm 2.1\%$  compared to  
323  $93.15\% \pm 6.1\%$  for (F3) ( $p < 0.01$ ). This might be attributed to the inability of phospholipid  
324 structure to entrap this high amount of peptide inside its aqueous drug layers [52].

325 *In vitro* release profiles and the initial burst release were closely related to the degree of  
326 peptide loading (Fig.1B). The burst release of F3 with peptide loading of 3% w/w was  
327 significantly lower than those of (F9) with 7% peptide loading ( $p < 0.01$ ). Initial bursts of  
328  $44.7\% \pm 5.7\%$ ,  $56.2\% \pm 6.1\%$  and  $65.9\% \pm 4.2\%$  were observed from F3, F6 and F9,  
329 respectively. High peptide loading in the dispersion medium enhanced the saturation of  
330 liposomal structure with peptide creating a relatively higher concentration gradient driving  
331 a higher rate of diffusion of peptide towards the external aqueous release phase increasing  
332 burst and total *in vitro* release [53].

333 According to the previous results, it was clear that F3 was found to be the optimum peptide-  
334 loaded liposome formulation as it has the lowest size, highest zeta potential, highest  
335 encapsulation efficiency, and lowest initial burst release. Therefore, the same formulation  
336 conditions adopted for preparing (F3) were used for co-encapsulation of peptide and DOX  
337 in the same liposome to prepare (double-loaded liposome).

338

### 339 *3.3. Effect of adding DOX*

340 In this part of the study, DOX was dissolved along with the NT 3-12 peptide in the same  
341 aqueous dispersion medium of (PBS, pH 7.4) to investigate the effect of adding DOX on  
342 the physicochemical characterization of different peptide-loaded liposomes (Table 2). The  
343 addition of DOX to peptide-loaded liposomes as in the case of (F11) demonstrated no  
344 significant increase of the mean liposome size compared to (F3) prepared without Dox ( $p$   
345  $> 0.05$ ). A significant decrease in zeta potential was observed ( $p < 0.05$ ). A slight decrease  
346 in peptide % E.E was observed. On the other hand, the % E.E of doxorubicin was 80.6%.  
347 Nonetheless, a significant increase in the initial burst release of the peptide was also  
348 observed ( $p < 0.05$ ) (Fig. 1.C). This might be attributed to the displacement effect of the  
349 loaded DOX on the loaded peptide resulting in lower encapsulation efficiency and higher  
350 initial release [54]. Approximately, 58% of peptide was released after 24 h which  
351 accounted for the drug adsorbed on the surface of the liposomes. However, 99 % of peptide  
352 was released after 72 h, due to the drug encapsulated inside the inner aqueous core of the  
353 dual-loaded liposomes. These results indicated the presence of drug in both adsorbed form  
354 and encapsulated. On the other hand, DOX showed a different release profile with a  
355 significantly lower initial burst release ( $p < 0.01$ ) of 35.7% compared to 58.6 % of peptide

356 released from F11. Faster DOX release was observed after the first 24 hours with almost  
357 97.3% released after 48 hours. The fast release of DOX after 24 hours may be due to high  
358 diffusion of the encapsulated drug towards the dissolution media depending on its small  
359 molecular weight compared to the high molecular weight of the encapsulated peptide. In  
360 addition, membrane fluidity of the prepared liposomes might contribute to the high DOX  
361 release. Incorporation of DOPE with low phase transition temperature  $T_c$  of -16 increased  
362 the fluidity of the liposomal membrane which facilitated doxorubicin release[55]. *In vitro*  
363 release, results showed that peptide and Dox can be released efficiently from the dual  
364 loaded liposomal carrier.

365 Based on the above results, F11 was used for further *in vitro* and *in vivo* experiments due  
366 to its superior physiochemical properties compared to other formulations as demonstrated  
367 by its optimum mean size, zeta potential, encapsulation efficiency and *in vitro* release of  
368 both drugs.

369

#### 370 ***3.4. Transmission electron microscopy***

371 To visualize the surface morphology of the double-loaded liposome (F11), TEM was used  
372 to assess the liposome morphology. TEM images revealed a smooth spherical shape of  
373 homogenous size, with no evidence of liposome adhesion or aggregation (Fig. 2.A). The  
374 average size obtained using TEM showed no significant differences when compared to  
375 similar data captured using light scattering.

376 To ensure the stability of this formulation (F11), a sample was stored in a fridge at 4°C for  
377 4 weeks and its particle size was measured periodically. The results show that the particle  
378 size showed a non-significant increase after 3 weeks compared to freshly prepared

379 liposomes ( $p > 0.05$ ). A significant increase in liposomal size ( $p < 0.05$ ) was noticed on  
380 day 28 after preparation (Fig 2.B). The % E.E of both peptide and doxorubicin showed a  
381 non-significant change after 5 days of preparations ( $p > 0.05$ ). Therefore, freshly prepared  
382 samples were used continuously for *in vivo* study.

383

### 384 **3.5. *In vitro* cell viability assay**

385 The cytotoxic action of different liposomal treatments on the MDA-MB 231, MCF-7, and  
386 A549 cell lines were evaluated by MTT assay 24, 48, and 72 hours after treatment (Fig. 3).  
387 MDA-MB 231 and MCF-7 breast cancer cell lines were used efficiently as a model for  
388 studying doxorubicin resistance[56]. Besides, A549 cell line is one of resistant lung cell  
389 lines against doxorubicin treatment[57]. The results show that the blank liposome and free  
390 peptide had no cytotoxicity on breast and lung cancer cells. Treatment with peptide-loaded  
391 liposome (1 $\mu$ M) showed a significant reduction in cell viability compared to the control  
392 and free peptide ( $p < 0.05$ ). This confirms the subcellular delivery of peptide inside the  
393 cancer cell where it can achieve its action on Ran inactivation as we previously reported  
394 [23,31]. On the other hand, treatment with free DOX and DOX-loaded liposomes showed  
395 a significant reduction in cell viability compared to control cells ( $p < 0.05$ ). However,  
396 treatment with DOX-loaded liposome showed more cytotoxic action compared to the free  
397 drug ( $p < 0.01$ ). These results were in good agreement with other previously reported [58].  
398 The dose-effect curves were plotted to measure the liposomal drug concentration that  
399 caused 50% growth inhibition ( $IC_{50}$ ). Double-loaded liposome (F11) showed a dose-  
400 dependent cytotoxic action in all cell lines as cell viability decreased with increasing the  
401 dose from 0.25 to 1  $\mu$ M. Treatment of MDA-MB 231 breast cancer cells with double-

402 loaded liposome reduced cell viability in a dose-dependent manner while maintaining its  
403 cytotoxic action up to three days after treatment due to sustained cytotoxic action (Fig.  
404 3.A). After 24 hours of treatment, the mean  $IC_{50}$  value of double-loaded liposome (F11) in  
405 MDA-MB 231 cells was  $0.304 \pm 0.08 \mu\text{M}$ . This  $IC_{50}$  value is significantly lower than  
406 previously calculated  $IC_{50}$  of our peptide-loaded polymeric nanoparticles which was  
407 estimated to be  $3.6 \mu\text{M}$  ( $p < 0.001$ ) [31]. This might be due to the co-delivery of DOX and  
408 peptide together in the same liposome as well as to the nature of the liposomes as a superior  
409 drug delivery vehicle. Higher cytotoxic action was observed after the treatment of MCF-7  
410 breast cancer cells with double-loaded liposomes. A similar dose-dependent effect was  
411 demonstrated in the case of MCF-7 cells. The mean  $IC_{50}$  value of (F11) in the case of MCF-  
412 7 cells was  $0.112 \pm 0.05 \mu\text{M}$ , which was significantly lower than  $IC_{50}$  of the same treatment  
413 in MDA-MB 231 cells calculated after 24 hours ( $p < 0.01$ ) (Fig. 3.B). Treatment of lung  
414 cancer cells with (F11) showed a similar dose-dependent cytotoxic action up for three days  
415 after treatment (Fig. 3.C). The mean  $IC_{50}$  value for (F11) in A549 cells was  $0.416 \pm 0.12$   
416  $\mu\text{M}$ , compared to similar  $IC_{50}$  values for MDA-MB 231 and MCF-7, respectively ( $p <$   
417  $0.05$ ). Cell viability results showed a non-significant decrease in cell viability after 72 hours  
418 compared to 48 hours ( $p > 0.05$ ) especially in lung cancer cells. This might be attributed to  
419 cell saturation with both drugs. Besides, *in vitro* release results showed a non-significant  
420 difference between the amount of peptide and doxorubicin released after 48 and 72 hours  
421 from the double-loaded liposomes.

422 Based on these results, double-loaded liposome (F11) achieved a significant reduction in  
423 cell viability ( $p < 0.001$ ) compared to free peptide, peptide-loaded liposome, free DOX,  
424 and DOX-loaded liposome. Besides, F11 showed a significant cytotoxic action compared

425 to the combination of both peptide-loaded and DOX-loaded liposomes. This might be  
426 attributed to the synergistic anti-cancer effect resulted from the co-delivery of peptide and  
427 DOX in one liposomal form. Double-loaded liposome achieved successful peptide and  
428 DOX delivery to the subcellular site of action meanwhile preserving their anti-cancer  
429 activity after formulation.

430

### 431 ***3.6. Quantitative Real-time PCR***

432 To explain the results of the cell viability study, qPCR was carried out to investigate the  
433 effect of Dox on mRNA ran expression. The results were analysed as mean  $\pm$  SD by use of  
434 analysis of variance (ANOVA) with Dunnett's multiple comparisons test using GraphPad  
435 prism 8.1.2. (Fig. 4.A) shows RAN mRNA expression level in MDA-MB-231 cell-line  
436 following treatment with Dox 1 $\mu$ M at three-time points (6,12 and 24h). RAN mRNA  
437 expression was downregulated after 6 and 12 hours treated by 1 $\mu$ M Dox by 40% and 20%,  
438 respectively compared to control empty liposome treated cells. This could be due to a  
439 decrease in cell viability.

440 At 24 hours, however, the level of Ran mRNA expression was significantly increased by  
441 100% compared to the control and by 200% compared to the 6hrs level. Following the  
442 treatment of MDA-MB231 cell by Dox at 1.3  $\mu$ M, Ran mRNA expression was decreased  
443 by 20% at 6 hours compared to empty liposome treated cells but increased at 12 and 24 hrs  
444 to 110% and 200%, respectively compared to the cells treated by empty liposome. The  
445 addition of the liposomal RAN-GTP blockade peptide counteracted the overexpression in  
446 RAN mRNA due to the treatment with DOX (Fig. 4.B).

447 Ran overexpression may help cancer cells resistance to DOX. It has been shown that Ran  
448 has an important role in DNA damage repair, thus introducing a RAN inhibitor will  
449 neutralize this effect and synergize the effect of DNA damage caused by DOX and, thus,  
450 increase cell apoptosis. *In vitro* results showed that DOX inhibited RAN expression in cells  
451 then after 24 hours RAN expression was upregulated hence cells are resisting the cytotoxic  
452 effect of DOX. The after treating with RAN-IP, the RAN expression was downregulated  
453 again and re-sensitize the cells to DOX.

454

### 455 **3.7. *In vivo* studies**

#### 456 **3.7.1. *In vivo* antitumor efficacy**

457 This study was performed using the SEC model to investigate the anti-cancer activity of  
458 prepared nano-drug delivery systems on breast cancer-induced in mice. The SEC model  
459 was carefully selected for this study due to the following reasons. Firstly, SEC is a well-  
460 established murine mammary adenocarcinoma model in tumor biology. This model has  
461 largely been used for study of tumor pathogenesis and development of anti-tumorigenic  
462 agents[59]. Secondly, the Ehrlich model is used extensively in studying the MDR of  
463 different chemotherapeutics such as daunorubicin, Mitoxantrone, etoposide[60-62].  
464 Finally, Doxorubicin has been shown to induce expression of P-gp after only 24 h of  
465 contact with sensitive Ehrlich cells[61,63,64]. Therefore, this model can develop MDR to  
466 doxorubicin in a very short time of only 24 hours[63], meanwhile, the duration of our *in*  
467 *vivo* study was 16 days. The antitumor activity of peptide-loaded liposome, Dox-loaded  
468 liposome, and double-loaded liposome (Table 3) was demonstrated in (Fig. 5).  
469 Intraperitoneal administration (IP) of liposomal drug delivery systems was selected due to

470 its numerous advantages. Previous studies showed that, intraperitoneal administration of  
471 siRNA-loaded liposomes was as efficient as intravenous administration for treatment of  
472 ovarian cancer. Liposomes injected IP were distributed by diffusion into intraperitoneal  
473 cavity through the vasculature, rather than direct diffusion to reach the tumor site from the  
474 peritoneal cavity[65]. IP administration of doxorubicin-loaded liposome was the best  
475 choice for treatment of SEC model *in vivo* due to its significant effect on prolongation of  
476 survival time of treated animals due to its leaky properties and high peritoneal  
477 dissemination of these liposomes[66]. After 16 days of treatment, the control and blank  
478 liposome-treated groups showed an increase in tumor volume by 281.93% and 312.25%,  
479 respectively. Animals treated with free peptide (10 mg kg<sup>-1</sup>) showed no anti-tumor activity  
480 as tumor volumes increased by 354.24%. Mice treated by peptide-loaded liposome (10 mg  
481 kg<sup>-1</sup>), free DOX (5 mg kg<sup>-1</sup>) and DOX liposome (5 mg kg<sup>-1</sup>) exhibited a significant tumour  
482 growth inhibition of 55.4%, 50.22% and 65.91% respectively (p < 0.001) (Fig. 6). The  
483 animal group treated with the combination of peptide liposome (10 mg kg<sup>-1</sup>) and DOX  
484 liposome (5 mg kg<sup>-1</sup>) demonstrated a 78.61% reduction in tumor volume that was  
485 significantly more effective than the use of each single-drug loaded liposome (p < 0.001).  
486 Treatment with double-loaded liposomes showed the highest % of tumor growth inhibition  
487 of 85.91%, 95.55%, and 97.77% in cases of 1X, 2X, and 3X, respectively. The most  
488 favourable antitumor activity was observed in animals treated with double-loaded  
489 liposomes (2X and 3X). These results confirm the superiority of synergistically combined  
490 therapy of NT 3-12 peptide and DOX. This is the first time to report the anticancer activity  
491 of the combination of NT 3-12 peptide and DOX by co-delivery of both drugs in a  
492 liposome-based drug delivery system.

493 At the end of the treatment, all animals were sacrificed. A photograph of excised tumors  
494 for each animal group was shown in (Fig. 7). The difference in tumor weights between  
495 control and treated animals was exhibited in (Fig. 8). The average tumor weight in the  
496 control group after treatment was  $3.95 \pm 0.46$  g. Animals treated with double-loaded  
497 liposomes showed a reduction in average tumor weight of 91.13 %, 97.46%, and 99.49%  
498 in cases of 1X, 2X, and 3X, respectively ( $p < 0.001$ ).

499

### 500 **3.7.2. *In vivo* safety**

501 There were no signs of decreased activity or abnormal behaviour, which indicates no  
502 toxicity caused by all treatments. Most animals appeared healthy and no substantial body  
503 weight loss was observed (Fig. 9). However, animals treated with free DOX and DOX-  
504 loaded liposomes showed a significant body weight loss compared to the control animal ( $p$   
505  $< 0.05$ ). Biochemical assays were done to investigate the cardiotoxicity of DOX-loaded  
506 liposome *in vivo*. Three different biochemical parameters of cardiac MDA, LDH, and CK-  
507 MB levels were investigated, and results were presented in (Table 4). Tumor-bearing  
508 animals served as a control group showed a non-significant ( $P > 0.05$ ) increase in cardiac  
509 MDA compared to normal animals. Mice treated with free DOX and DOX-loaded  
510 liposome showed a significant increase in cardiac MDA levels compared to control animals  
511 and animals treated with peptide-loaded liposome. However, DOX-loaded liposome  
512 showed a non-significant decrease in MDA level compared to free DOX. This was due to  
513 the cardiotoxic effect of DOX *in vivo*. Besides, treatment with free DOX and DOX-loaded  
514 liposomes resulted in a significant increase in LDH and CK-MB activity levels. However,  
515 DOX-loaded liposome showed a significant decrease in CK-MB level compared to free

516 DOX treated animals ( $p < 0.05$ ). Fortunately, double-loaded liposomes showed a non-  
517 significant increase in cardiac MDA, LDH, and CK-MB levels compared to control  
518 animals which can confirm its safety for *in vivo* use.

519

520

#### 521 **4. Conclusions**

522 Peptide-loaded liposomes were prepared using a thin film rehydration technique  
523 comprising several peptides and DOX loading levels, and variable pH of the dispersion  
524 media. An optimum double-loaded liposome was selected, which had the highest peptide  
525 loading of 85%, the lowest particle size of 80 nm, whilst sustaining the peptide and Dox  
526 release for 3 days. *In vitro* cell viability studies of peptide-loaded liposomes showed  
527 superior cytotoxic action compared to free peptide and free Dox. The highest reduction in  
528 cell viability was observed in case of MCF-7 due to the lowest IC<sub>50</sub> of  $0.112 \pm 0.05$   
529 compared to  $0.304 \pm 0.08$  and  $0.416 \pm 0.12 \mu\text{M}$  for MDA-MB-231 and A549, respectively  
530 after treatment with double-loaded liposome. Dox treatment was shown to cause a  
531 significant increase in RanGTP mRNA level, and this increase was successfully reversed  
532 when RAN-IP was included in the treatment. The *in vivo* results confirmed the enhanced  
533 anti-cancer activity of double-loaded liposome by achieving 85.91%, 95.55%, and 97.77%  
534 tumor growth inhibition after treatment with different doses of 1X, 2X and 3X of the  
535 double-loaded liposome. Toxicity examinations showed that a combined-drug delivery  
536 system was found to be safer to liver and kidney tissues when compared to the free DOX.  
537 The emergence of a novel drug delivery system is of high clinical importance because it  
538 will improve the therapeutic response by providing a synergistic anti-tumor effect both *in*  
539 *vitro* and *in vivo* along with causing minimal side effects compared to classic dosage forms  
540 of the same drugs.

541

## 542 **References**

- 543 1. Merlo LM, Pepper JW, Reid BJ, et al. Cancer as an evolutionary and ecological process.  
544 Nature reviews Cancer. 2006 Dec;6(12):924-35.
- 545 2. Siegel RL, Miller KD, Jemal A. Cancer statistics, 2019. CA: a cancer journal for clinicians.  
546 2019 Jan;69(1):7-34.
- 547 3. Atkins MB, Tannir NM. Current and emerging therapies for first-line treatment of  
548 metastatic clear cell renal cell carcinoma. Cancer treatment reviews. 2018 Nov;70:127-  
549 137.
- 550 4. Haffty BG, Yang Q, Reiss M, et al. Locoregional relapse and distant metastasis in  
551 conservatively managed triple negative early-stage breast cancer. Journal of clinical  
552 oncology : official journal of the American Society of Clinical Oncology. 2006 Dec  
553 20;24(36):5652-7.
- 554 5. Dawar S, Singh N, Kanwar RK, et al. Multifunctional and multitargeted nanoparticles for  
555 drug delivery to overcome barriers of drug resistance in human cancers. Drug Discov  
556 Today. 2013 Dec;18(23-24):1292-300.
- 557 6. Coley HM. Mechanisms and strategies to overcome chemotherapy resistance in  
558 metastatic breast cancer. Cancer Treat Rev. 2008 Jun;34(4):378-90.
- 559 7. Szakacs G, Hall MD, Gottesman MM, et al. Targeting the Achilles heel of multidrug-  
560 resistant cancer by exploiting the fitness cost of resistance. Chem Rev. 2014 Jun  
561 11;114(11):5753-74.
- 562 8. Markman JL, Rekechenetskiy A, Holler E, et al. Nanomedicine therapeutic approaches to  
563 overcome cancer drug resistance. Advanced drug delivery reviews. 2013 Nov;65(13-  
564 14):1866-79.
- 565 9. Minotti G, Menna P, Salvatorelli E, et al. Anthracyclines: molecular advances and  
566 pharmacologic developments in antitumor activity and cardiotoxicity. Pharmacol Rev.  
567 2004 Jun;56(2):185-229.
- 568 10. Minotti G, Recalcati S, Menna P, et al. Doxorubicin cardiotoxicity and the control of iron  
569 metabolism: quinone-dependent and independent mechanisms. Methods Enzymol.  
570 2004;378:340-61.
- 571 11. Capelôa T, Benyahia Z, Zampieri LX, et al. Metabolic and non-metabolic pathways that  
572 control cancer resistance to anthracyclines. Seminars in cell & developmental biology.  
573 2020 Feb;98:181-191.
- 574 12. Aas T, Børresen A-L, Geisler S, et al. Specific P53 mutations are associated with de novo  
575 resistance to doxorubicin in breast cancer patients. Nature Medicine. 1996  
576 1996/07/01;2(7):811-814.
- 577 13. Loi S, Pommey S, Haibe-Kains B, et al. CD73 promotes anthracycline resistance and poor  
578 prognosis in triple negative breast cancer. Proceedings of the National Academy of  
579 Sciences of the United States of America. 2013 Jul 2;110(27):11091-6.
- 580 14. Shen J, He Q, Gao Y, et al. Mesoporous silica nanoparticles loading doxorubicin reverse  
581 multidrug resistance: performance and mechanism. Nanoscale. 2011 Oct 5;3(10):4314-  
582 22.
- 583 15. Iyer AK, Singh A, Ganta S, et al. Role of integrated cancer nanomedicine in overcoming  
584 drug resistance. Advanced drug delivery reviews. 2013 Nov;65(13-14):1784-802.
- 585 16. Turner JG, Dawson J, Sullivan DM. Nuclear export of proteins and drug resistance in  
586 cancer. Biochemical Pharmacology. 2012;83(8):1021-1032.

- 587 17. Nielsen D, Maare C, Poulsen F, et al. The relationship between resistance, P-glycoprotein  
588 content, and steady state accumulation in five series of Ehrlich ascites tumor cell lines  
589 selected for resistance to daunorubicin. *Cell Pharmacol.* 1994;1:127-135.
- 590 18. Zununi Vahed S, Salehi R, Davaran S, et al. Liposome-based drug co-delivery systems in  
591 cancer cells. *Materials Science and Engineering: C.* 2017 2017/02/01/;71:1327-1341.
- 592 19. Torchilin V, Weissig V. *Liposomes: a practical approach.* Oxford University Press; 2003.  
593 (264).
- 594 20. Bulbake U, Doppalapudi S, Kommineni N, et al. *Liposomal Formulations in Clinical Use: An  
595 Updated Review.* *Pharmaceutics.* 2017;9(2):12.
- 596 21. Chen X, Wang X, Wang Y, et al. Improved tumor-targeting drug delivery and therapeutic  
597 efficacy by cationic liposome modified with truncated bFGF peptide. *Journal of controlled  
598 release : official journal of the Controlled Release Society.* 2010 Jul 1;145(1):17-25.
- 599 22. Sercombe L, Veerati T, Moheimani F, et al. *Advances and Challenges of Liposome Assisted  
600 Drug Delivery.* *Frontiers in pharmacology.* 2015;6:286-286.
- 601 23. Haggag YA, Matchett KB, Falconer RA, et al. *Novel Ran-RCC1 Inhibitory Peptide-Loaded  
602 Nanoparticles Have Anti-Cancer Efficacy In Vitro and In Vivo.* *Cancers.* 2019 Feb 14;11(2).
- 603 24. Kurisetty VV, Johnston PG, Johnston N, et al. RAN GTPase is an effector of the  
604 invasive/metastatic phenotype induced by osteopontin. *Oncogene.* 2008 Dec  
605 04;27(57):7139-49.
- 606 25. Yuen HF, Chan KK, Grills C, et al. Ran is a potential therapeutic target for cancer cells with  
607 molecular changes associated with activation of the PI3K/Akt/mTORC1 and Ras/MEK/ERK  
608 pathways. *Clin Cancer Res.* 2012 Jan 15;18(2):380-91.
- 609 26. Clarke PR, Zhang C. Spatial and temporal coordination of mitosis by Ran GTPase. *Nat Rev  
610 Mol Cell Biol.* 2008 Jun;9(6):464-77.
- 611 27. Yuen H-F, Chan K-K, Platt-Higgins A, et al. Ran GTPase promotes cancer progression via  
612 Met receptormediated downstream signaling. 2016. (2016).
- 613 28. Yuen HF, Gunasekharan VK, Chan KK, et al. RanGTPase: a candidate for Myc-mediated  
614 cancer progression. *Journal of the National Cancer Institute.* 2013 Apr 3;105(7):475-88.
- 615 29. Cekan P, Hasegawa K, Pan Y, et al. RCC1-dependent activation of Ran accelerates cell cycle  
616 and DNA repair, inhibiting DNA damage-induced cell senescence. *Mol Biol Cell.* 2016 Apr  
617 15;27(8):1346-57.
- 618 30. Cekan P, Hasegawa K, Pan Y, et al. RCC1-dependent activation of Ran accelerates cell cycle  
619 and DNA repair, inhibiting DNA damage-induced cell senescence. *Molecular biology of  
620 the cell.* 2016;27(8):1346-1357.
- 621 31. Haggag YA, Matchett KB, Dakir El H, et al. Nano-encapsulation of a novel anti-Ran-GTPase  
622 peptide for blockade of regulator of chromosome condensation 1 (RCC1) function in  
623 MDA-MB-231 breast cancer cells. *International journal of pharmaceutics.* 2017 Apr  
624 15;521(1-2):40-53.
- 625 32. Lei M, Ma G, Sha S, et al. Dual-functionalized liposome by co-delivery of paclitaxel with  
626 sorafenib for synergistic antitumor efficacy and reversion of multidrug resistance. *Drug  
627 delivery.* 2019;26(1):262-272.
- 628 33. Zhang Y, Zhai M, Chen Z, et al. Dual-modified liposome codelivery of doxorubicin and  
629 vincristine improve targeting and therapeutic efficacy of glioma. *Drug delivery.* 2017  
630 2017/01/01;24(1):1045-1055.
- 631 34. Lakkadwala S, dos Santos Rodrigues B, Sun C, et al. Dual functionalized liposomes for  
632 efficient co-delivery of anti-cancer chemotherapeutics for the treatment of glioblastoma.  
633 *Journal of Controlled Release.* 2019 2019/08/10/;307:247-260.

- 634 35. Ierano C, Portella L, Lusa S, et al. CXCR4-antagonist Peptide R-liposomes for combined  
635 therapy against lung metastasis. *Nanoscale*. 2016 Apr 14;8(14):7562-71.
- 636 36. Roy B, Guha P, Bhattarai R, et al. Influence of Lipid Composition, pH, and Temperature on  
637 Physicochemical Properties of Liposomes with Curcumin as Model Drug. *Journal of oleo*  
638 *science*. 2016;65(5):399-411.
- 639 37. Dharmalingam SR, Ramamurthy S, Chidambaram K, et al. A simple HPLC bioanalytical  
640 method for the determination of doxorubicin hydrochloride in rat plasma: application to  
641 pharmacokinetic studies. *Tropical journal of pharmaceutical research*. 2014;13(3):409-  
642 415.
- 643 38. Haggag YA, Ibrahim RR, Hafiz AA. Design, Formulation and in vivo Evaluation of Novel  
644 Honokiol-Loaded PEGylated PLGA Nanocapsules for Treatment of Breast Cancer.  
645 *International journal of nanomedicine*. 2020;15:1625-1642.
- 646 39. Haggag Y, Elshikh M, El-Tanani M, et al. Nanoencapsulation of sophorolipids in PEGylated  
647 poly(lactide-co-glycolide) as a novel approach to target colon carcinoma in the murine  
648 model. *Drug Deliv Transl Res*. 2020 Apr 1.
- 649 40. Haggag Y, Elshikh M, El-Tanani M, et al. Nanoencapsulation of sophorolipids in PEGylated  
650 poly(lactide-co-glycolide) as a novel approach to target colon carcinoma in the murine  
651 model. *Drug Delivery and Translational Research*. 2020 2020/04/01.
- 652 41. Yuen HF, Chan KK, Platt-Higgins A, et al. Ran GTPase promotes cancer progression via Met  
653 receptormediated downstream signaling. *Oncotarget*. 2016 Oct 03.
- 654 42. Haggag YA, Osman MA, El-Gizawy SA, et al. Polymeric nano-encapsulation of 5-  
655 fluorouracil enhances anti-cancer activity and ameliorates side effects in solid Ehrlich  
656 Carcinoma-bearing mice. *Biomedicine & Pharmacotherapy*. 2018;105:215-224.
- 657 43. Papadopoulos D, Kimler BF, Estes NC, et al. Growth delay effect of combined interstitial  
658 hyperthermia and brachytherapy in a rat solid tumor model. *Anticancer research*. 1989  
659 Jan-Feb;9(1):45-7.
- 660 44. Yoshioka T, Kawada K, Shimada T, et al. Lipid peroxidation in maternal and cord blood and  
661 protective mechanism against activated-oxygen toxicity in the blood. *American journal of*  
662 *obstetrics and gynecology*. 1979 Oct 1;135(3):372-6.
- 663 45. Buhl SN, Jackson KY. Optimal conditions and comparison of lactate dehydrogenase  
664 catalysis of the lactate-to-pyruvate and pyruvate-to-lactate reactions in human serum at  
665 25, 30, and 37 degrees C. *Clinical chemistry*. 1978 May;24(5):828-31.
- 666 46. Rosalki SB. An improved procedure for serum creatine phosphokinase determination. *The*  
667 *Journal of Laboratory and Clinical Medicine*. 1967;69(4):696-705.
- 668 47. Zhang H. Thin-Film Hydration Followed by Extrusion Method for Liposome Preparation.  
669 *Methods in molecular biology (Clifton, NJ)*. 2017;1522:17-22.
- 670 48. Ai X, Zhong L, Niu H, et al. Thin-film hydration preparation method and stability test of  
671 DOX-loaded disulfide-linked polyethylene glycol 5000-lysine-di-tocopherol succinate  
672 nanomicelles. *Asian Journal of Pharmaceutical Sciences*. 2014 2014/10/01;9(5):244-250.
- 673 49. Garidel P, Johann C, Mennicke L, et al. The mixing behavior of pseudobinary  
674 phosphatidylcholine-phosphatidylglycerol mixtures as a function of pH and chain length.  
675 *European biophysics journal*. 1997;26(6):447-459.
- 676 50. Sułkowski W, Pentak D, Nowak K, et al. The influence of temperature, cholesterol content  
677 and pH on liposome stability. *Journal of Molecular Structure*. 2005;744:737-747.
- 678 51. Brgles M, Jurasin D, Sikiric MD, et al. Entrapment of ovalbumin into liposomes--factors  
679 affecting entrapment efficiency, liposome size, and zeta potential. *Journal of liposome*  
680 *research*. 2008;18(3):235-48.

- 681 52. Chountoulesi M, Naziris N, Pippa N, et al. The significance of drug-to-lipid ratio to the  
682 development of optimized liposomal formulation. *Journal of liposome research*. 2018  
683 Sep;28(3):249-258.
- 684 53. Johnston MJ, Edwards K, Karlsson G, et al. Influence of drug-to-lipid ratio on drug release  
685 properties and liposome integrity in liposomal doxorubicin formulations. *Journal of*  
686 *liposome research*. 2008;18(2):145-57.
- 687 54. Tefas LR, Sylvester B, Tomuta I, et al. Development of antiproliferative long-circulating  
688 liposomes co-encapsulating doxorubicin and curcumin, through the use of a quality-by-  
689 design approach. *Drug design, development and therapy*. 2017;11:1605.
- 690 55. Li J, Wang X, Zhang T, et al. A review on phospholipids and their main applications in drug  
691 delivery systems. *Asian Journal of Pharmaceutical Sciences*. 2015 2015/04/01;/10(2):81-  
692 98.
- 693 56. Marinello PC, Panis C, Silva TNX, et al. Metformin prevention of doxorubicin resistance in  
694 MCF-7 and MDA-MB-231 involves oxidative stress generation and modulation of cell  
695 adaptation genes. *Scientific Reports*. 2019 2019/04/10;9(1):5864.
- 696 57. Xu L, Li H, Wang Y, et al. Enhanced activity of doxorubicin in drug resistant A549 tumor  
697 cells by encapsulation of P-glycoprotein inhibitor in PLGA-based nanovectors. *Oncol Lett*.  
698 2014;7(2):387-392.
- 699 58. Lao J, Madani J, Pu, et al. Liposomal Doxorubicin in the Treatment of Breast Cancer  
700 Patients: A Review. *Journal of Drug Delivery*. 2013;2013:12.
- 701 59. Mishra S, Tamta AK, Sarikhani M, et al. Subcutaneous Ehrlich Ascites Carcinoma mice  
702 model for studying cancer-induced cardiomyopathy. *Scientific reports*. 2018;8(1):5599-  
703 5599.
- 704 60. Nielsen D, Maare C, Eriksen J, et al. Characterisation of multidrug-resistant Ehrlich ascites  
705 tumour cells selected in vivo for resistance to etoposide. *Biochemical pharmacology*. 2000  
706 Aug 1;60(3):353-61.
- 707 61. Nielsen D, Eriksen J, Maare C, et al. P-glycoprotein expression in Ehrlich ascites tumour  
708 cells after in vitro and in vivo selection with daunorubicin. *British journal of cancer*. 1998  
709 Nov;78(9):1175-80.
- 710 62. Nielsen D, Eriksen J, Maare C, et al. Characterisation of non-P-glycoprotein multidrug-  
711 resistant Ehrlich ascites tumour cells selected for resistance to mitoxantrone. *Biochemical*  
712 *pharmacology*. 2000 Aug 1;60(3):363-70.
- 713 63. Volm M, Mattern J, Pommerenke E. Time course of MDR gene amplification during in vivo  
714 selection for doxorubicin-resistance and during reversal in murine leukemia L 1210.  
715 *Anticancer research*. 1991;11(2):579.
- 716 64. Chevillard S, Vielh P, Bastian G, et al. A single 24h contact time with adriamycin provokes  
717 the emergence of resistant cells expressing the Gp 170 protein. *Anticancer research*.  
718 1992;12(2):495-499.
- 719 65. Landen CN, Merritt WM, Mangala LS, et al. Intraperitoneal delivery of liposomal siRNA for  
720 therapy of advanced ovarian cancer. *Cancer biology & therapy*. 2006;5(12):1708-1713.
- 721 66. Sadzuka Y, Hirama R, Sonobe T. Effects of intraperitoneal administration of liposomes and  
722 methods of preparing liposomes for local therapy. *Toxicology letters*. 2002 Jan  
723 25;126(2):83-90.

724

725

726